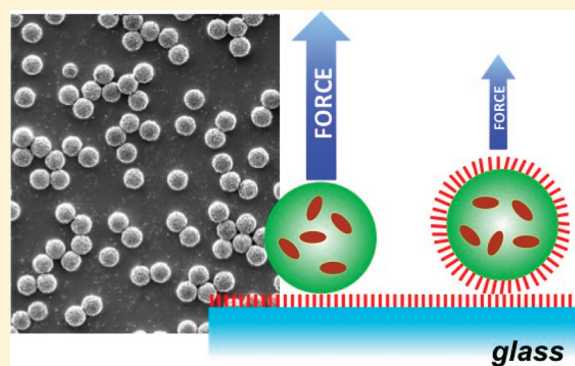


## Coatings of Polyethylene Glycol for Suppressing Adhesion between Solid Microspheres and Flat Surfaces

Srigokul Upadhyayula,<sup>†,‡,§</sup> Timothy Quinata,<sup>†,‡</sup> Stephen Bishop,<sup>†,⊥</sup> Sharad Gupta,<sup>†,‡</sup> Noah Ray Johnson,<sup>†,#</sup> Baharak Bahmani,<sup>†,‡</sup> Kliment Bozhilov,<sup>†,||</sup> Jeremy Stubbs,<sup>†</sup> Pamela Jreij,<sup>†,∇</sup> Pratima Nallagatla,<sup>†</sup> and Valentine I. Vullev<sup>\*,†,‡,§,||</sup>

<sup>†</sup>Department of Bioengineering, <sup>‡</sup>Center for Bioengineering Research, <sup>§</sup>Department of Biochemistry, and <sup>⊥</sup>Department of Chemistry, University of California, Riverside, California 91521, United States

**ABSTRACT:** This article describes the development and the examination of surface coatings that suppress the adhesion between glass surfaces and polymer microspheres. Superparamagnetic doping allowed for exerting magnetic forces on the microbeads. The carboxyl functionalization of the polymer provided the means for coating the beads with polyethylene glycol (PEG) with different molecular weight. Under gravitational force, the microbeads settled on glass surfaces with similar polymer coatings. We examined the efficacy of removing the beads from the glass surfaces by applying a pulling force of  $\sim 1.2$  pN. The percent beads remaining on the surface after applying the pulling force for approximately 5 s served as an indication of the adhesion propensity. Coating of PEG with molecular weight ranging between 3 and 10 kDa was essential for suppressing the adhesion. For the particular substrates, surface chemistry and aqueous media we used, coatings of 5 kDa manifested optimal suppression of adhesion: that is, only 3% of the microbeads remained on the surface after applying the pulling magnetic force. When either the glass or the beads were not PEGylated, the adhesion between them was substantial. Addition of a noncharged surfactant, TWEEN, above its critical micelle concentrations (CMCs) suppressed the adhesion between noncoated substrates. The extent of this surfactant-induced improvement of the adhesion suppression, however, did not exceed the quality of preventing the adhesion that we attained by PEGylating both substrates. In addition, the use of surfactants did not significantly improve the suppression of bead-surface adhesion when both substrates were PEGylated. These findings suggest that such surfactant additives tend to be redundant and that covalently grafted coatings of PEGs with selected chain lengths provide sufficient suppression of nonspecific interfacial interactions.



### INTRODUCTION

Recent advances in single-molecule force measurements (SMFMs) provide the means to study and elucidate the intricacies of mechanisms and interactions within macromolecular structures.<sup>1,2</sup> As vital techniques, SMFMs allow for probing the energy landscape of bimolecular processes such as receptor–ligand interactions<sup>3</sup> and protein folding under mechanical stress.<sup>4</sup> The techniques for SMFM, such as biomembrane force probes, atomic force microscopes, and optical tweezers, have varying advantages and disadvantages. Among the array of SMFM tools available, we employed a variation of magnetic tweezers for their biocompatibility and force dynamic range. Magnetic forces are orthogonal to most biological interactions, and magnetic tweezers permit a reliable access to the low piconewton and subpiconewton force domain.

An effective way to experimentally study single-molecule mechanics is to employ force measurement on macromolecular complexes (with dimensions in the order of a few nanometers) immobilized on micrometer-size probes.<sup>2</sup> While the diffraction limit prohibits optical imaging of single molecules in their native environment, optical methods allow for tracking the

movement of micrometer-size probes, to which the molecules are connected, with ångström resolution. These probes (e.g., microbeads or AFM tips) have a dual purpose: (1) they are the force transducers and (2) they are the optical (imaging) probes for following mechanical displacements within the examined molecules.

Forces feasible for probing single-molecule interactions and conformational mechanics range between about 10 and 100 pN. This force domain, however, is overwhelmed by nonspecific interactions involving the micrometer-size probes. Nonspecific attractive forces (which result from van der Waals and other electric interactions)<sup>5,6</sup> between the probes and other solid interfaces readily exceed a nanonewton at nanometer separations, i.e., separations comparable to protein dimensions. In contrast, biospecific interactions involve the same forces in a spatially regulated and cooperative manner to ensure strong noncovalent binding only upon acceptable complementarity between the structure, the charge distribution,

Received: October 29, 2011

Published: February 24, 2012

and the hydrogen-bonding propensity of the interacting molecular species.<sup>5</sup> A principal challenge for SMFMs is characterizing such biospecific interactions, which are confined to a single molecule on the background of nonspecific attractive forces between probes that are orders of magnitude larger than the investigated molecule.

Coatings of physisorbed proteins are frequently the choice for suppressing nonspecific interactions.<sup>7</sup> The hydration and the charge similarity of the protein coatings provide nonspecific repellence, opposing the nonspecific van der Waals attraction between coated interfaces. Using such a passivation approach, however, is not optimal because it may preclude the study of proteins, materials, or macromolecules that interact with proteins.<sup>8</sup> Furthermore, the addition of surfactants may be a requirement for attaining adequate suppression of the undesired nonspecific adhesion between protein-coated interfaces.<sup>9,10</sup>

Surfactants, indeed, represent another widely used class of molecules for suppressing nonspecific interactions.<sup>11</sup> In order to be effective, however, these amphipaths are largely required in high concentrations, i.e., in concentrations exceeding their CMCs.<sup>12,13</sup> Additionally, the presence of surfactants in such high concentrations can disrupt active sites and, hence, the studied biospecific interactions, or worse, they can perturb the native protein structures.<sup>14</sup>

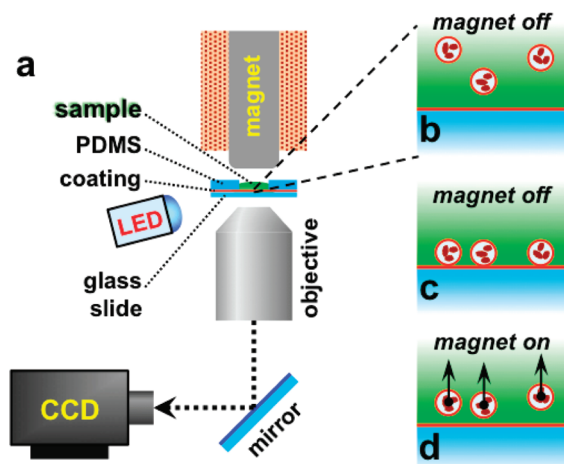
Therefore, it is essential to seek venues for suppressing the nonspecific interactions between micrometer-size objects when connected via nanometer-size molecules. Using chemisorbed (instead of physisorbed) passivation biocompatible coatings,<sup>15</sup> along with eliminating the need of additives such as surfactants, provides considerable advantages for SMFMs.

Herein, we demonstrated that covalently grafted coatings of polyethylene glycol (PEG), with a molecular weight (MW) considerably exceeding 1 kDa, suppressed the undesired adhesion of polymer microspheres to glass surfaces. We examined the adhesion propensity of polymer microspheres to flat glass surfaces when coated with PEGs with different length, varying from about 22 to 450 repeating units and corresponding to MW from about 1000 to 20 000 Da. (The PEGs with different MW are designated in the text as PEG-“MW in Da”, i.e., PEG-1000 to PEG-20000). Coatings of PEGs with MW ranging between 3 kDa and 10 kDa provided optimal suppression of the nonspecific adhesion. When the microbeads and the glass were coated with PEG-5000, less than 3% of the beads remained on the surface after applying 1.2 pN pulling force. When only the beads or the glass were coated (with PEG-3000), the nonspecific interactions were still prevalent. Adding a noncharged surfactant, TWEEN 20, only marginally improved the suppression of nonspecific interactions. Relating our adhesion findings with the structural features of the hydrated PEGs provided guidelines for suppressing nonspecific interactions between micrometer-size objects at nanometer separation.

## RESULTS

**Instrument Setup and Calibration.** We employed a variation of magnetic tweezers, more accurately termed magnetic pullers, in order to characterize the nonspecific interaction between glass surfaces and superparamagnetically doped polymer microspheres (Scheme 1). Magnetic pullers usually employ a single electromagnet that does not generate a magnetic trap. The pullers are relatively simple devices, and they allow for a well-controlled exertion of relatively weak

Scheme 1. Magnetic Tweezers/Puller<sup>a</sup>



<sup>a</sup>(a) Setup: the sample is a suspension of superparamagnetically doped microbeads, dropped on coated glass surfaces in wells of polydimethylsiloxane (PDMS), (b) gravity-driven settling of the beads, (c) beads settled on the glass surface, and (d) beads pulled off the surface.

forces on magnetic micro- and nano-objects, i.e., forces that are less than 10 pN, directed toward the magnet.

The magnetic pullers are inverted optical microscopes with electromagnets or permanent magnets above the sample focal plane (Scheme 1a).<sup>1</sup> Microbeads that contain paramagnetic material are allowed to settle under gravity on the surface of a sample slide. The surface on which the beads settle is within the depth of field of the objective (Scheme 1b). Magnetic field gradients, generated by the magnet above the focal plane, exert pulling forces on the beads (Scheme 1c). As the pulling force moves the microbeads away from the surface, and hence out of the depth of field, the beads “disappear” from the focus of the image. By recording movies of the beads settled in the field of depth,<sup>16,17</sup> we were able to monitor the number of beads on the glass surface at each time point.

We employed superparamagnetic materials to ensure that (1) the beads attain complete magnetization in relatively weak fields and (2) their magnetization would not manifest hysteretic behavior when the field was turned off. Hence, the magnitude of the force depended mostly on the field gradient, which was readily controlled by varying the current passed through the electromagnet coil or by moving the permanent magnet up and down above the focal plane.<sup>11,18</sup> Since we aimed at piconewton forces, we chose to employ an electromagnet in order to avoid moving parts and eliminate unnecessary vibrations during the measurements.

When suspended in the aqueous solution, each bead experienced  $\sim 0.3$  pN gravitational pull downward, as we determined from direct measurements and from calculations accounting for the bead buoyancy in the used media. After allowing the beads to settle on the glass surfaces for three minutes (Scheme 1c), we switched on the electromagnet to apply  $1.2 \pm 0.3$  pN upward net pulling force (Scheme 1d). We quantified the extent of the undesired adhesion as the percent of beads that remained on the surface after applying the magnetic force for 5 s (Figure 1).

In order to calibrate the magnetic puller, we moved the objective to attain a side view for the setup (Scheme 2). A suspension of the superparamagnetic microbeads was intro-

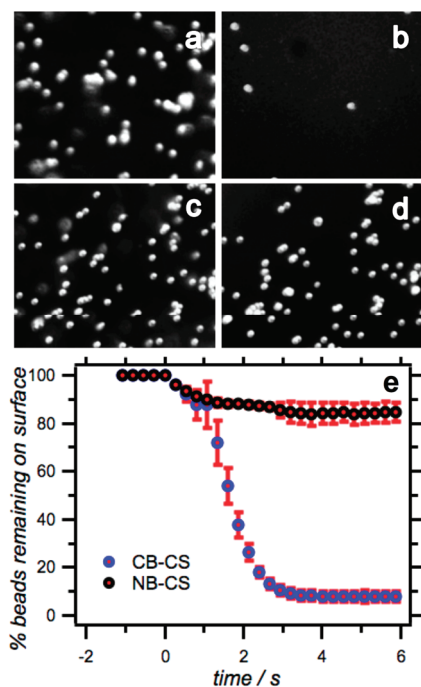
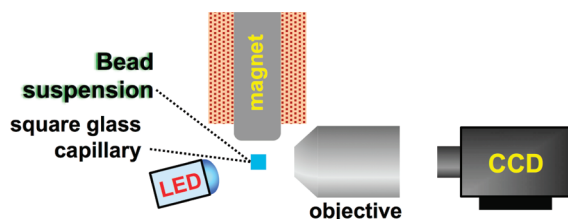


**Figure 1.** Removing of superparamagnetically doped polymer microbeads (3- $\mu\text{m}$  diameter) from glass surfaces using 1.2-pN net force. From a suspension in an aqueous solution (100 mM phosphate buffer, pH 7), the beads were allowed to settle for  $\sim 3$  min. (a–d) Reflection microscopy images of beads coated with PEG-3000 (a and b) on glass slides coated with PEG-3000 and (c and d) on noncoated glass slides; (a and c) after settling on the surface and before applying force, and (b and d) after applying magnetic force for 5 s. (e) Time course of desorption of beads from glass surfaces induced by 1.2-pN net force. (CB-CS designates coated beads settled on coated surfaces; and NB-CS designates noncoated beads settled on coated surfaces.) The beads were tracked while in focus. The depth of field of the used objective was 6  $\mu\text{m}$ , exceeding the bead size. Therefore, the beads were still in focus and tracked for a few seconds after desorption from the glass surface.

#### Scheme 2. Magnetic Tweezers/Puller in a Calibration Mode



duced in a square capillary under the magnet (Scheme 2). We recorded the velocities with which the microbeads in the capillary moved toward the magnet and employed the Stoke's drag equation for estimating the magnetic force on the beads at different distances from the magnet, and at various voltages applied to the coil of the electromagnet.

**Nonspecific Interfacial Interactions.** A range of interfacial attractive and repulsive forces governs the propensity for nonspecific adhesion of micrometer-size objects to solid surfaces.<sup>19,20</sup> As encompassed by the Derjaguin–Landau–Verwey–Overbeek (DLVO) theory, the double-layer electrostatic forces,  $F_{\text{DL}}$  (which can be attractive or repulsive), between a microsphere with a radius,  $r$ , and a flat solid surface decrease exponentially with the interfacial distance,  $d$ .<sup>6,19</sup> Concurrently,

the integrated van der Waals forces,  $F_{\text{vdW}}$  (which are inherently attractive), between a microsphere and a surface, nanometers away from the sphere, decrease with the square of  $d$  for small separation distances, i.e., for  $d \ll r$ .<sup>6,19</sup>

$$F_{\text{vdW}} = -\frac{Ar}{6d^2} \quad (1a)$$

$$F_{\text{DL}} = \kappa Zr \exp(-\kappa d) \quad (1b)$$

where  $A$  is the Hamaker constant taking into consideration the static,  $\epsilon_p$ , and dynamic,  $n_i^2$ , dielectric properties of the materials composing the sphere ( $i = 1$ ), the flat substrate ( $i = 2$ ), and the media separating the sphere from the flat surface ( $i = 3$ ).  $Z$  is a similar constant for the double-layer interactions that depends on the surface potential,  $\psi_0$ , and the valency of the electrolyte,  $z$ . The charge of the electrolyte ions,  $z_i$ , and their densities in the bulk solution,  $\rho_{\infty i}$  (i.e., at infinity  $d$ ), determine the Debye length,  $\kappa^{-1}$ , of the media with a relative dielectric constant  $\epsilon$ .<sup>6,19,21–25</sup>

$$\begin{aligned} A &= A_{\nu=0} + A_{\nu>0} \\ &\approx \frac{3}{4}k_{\text{B}}T \left( \frac{\epsilon_1 - \epsilon_3}{\epsilon_1 + \epsilon_3} \right) \left( \frac{\epsilon_2 - \epsilon_3}{\epsilon_2 + \epsilon_3} \right) + \frac{3}{8}h\nu_e \left[ (n_1^2 + n_3^2) \right. \\ &\quad \left. (n_2^2 + n_3^2) \right] / \left[ \left( \sqrt{n_1^2 + n_3^2} + \sqrt{n_2^2 + n_3^2} \right) \right. \\ &\quad \left. \sqrt{2(n_1^2 + n_3^2)(n_2^2 + n_3^2)} \right] \end{aligned} \quad (2a)$$

$$Z \approx 64\pi\epsilon_0\epsilon \left( \frac{k_{\text{B}}T}{e} \right)^2 \tanh^2 \left( \frac{ze\psi_0}{4k_{\text{B}}T} \right) \quad (2b)$$

$$\kappa = \sqrt{\frac{\sum_i \rho_{\infty i} (ez_i)^2}{\epsilon_0\epsilon k_{\text{B}}T}} \quad (2c)$$

where  $k_{\text{B}}$  is the Boltzmann constant,  $T$  is the thermodynamic temperature,  $\nu$  designates electromagnetic frequency, i.e.,  $A_{\nu=0}$  and  $A_{\nu>0}$  are the static and dynamic components of the Hamaker constant, respectively,  $\nu_e$  is a resonance electronic transition frequency (usually the band at the red edge of the UV/vis absorption spectra),  $h$  is the Planck constant,  $\epsilon_0$  is the electric permittivity of vacuum, and  $e$  is the elementary charge.

At distances exceeding about  $10\kappa^{-1}$ ,  $F_{\text{DL}}$  and  $F_{\text{vdW}}$  decrease to about a piconewton or less.<sup>6,26</sup> Considering, for example, the interactions between polymer microspheres and glass surfaces in aqueous media provided an estimate that an increase in  $d$  from about 1 to 30 nm decreased  $F_{\text{vdW}}$  3 orders of magnitude, i.e., from nanonewtons to piconewtons (eqs 1a and 2a). Thus, keeping tens of nanometers separation between the surfaces of the polymer microbeads and the glass may not be sufficient but is a necessary condition for preventing nonspecific adhesion.

Noncharged surface coatings bring the values of  $\psi_0$  close to zero. Therefore, for distances considerably exceeding the Debye length,  $|F_{\text{DL}}| \ll |F_{\text{vdW}}|$ . For the 100 mM phosphate buffer that we used in this study,  $\kappa \approx 1.3 \text{ nm}^{-1}$ , allowing us to ignore the contribution of the electrostatic (double layer) interactions between noncharged surfaces should the separation between the polymer and the glass exceed a few nanometers (eqs 1b, 2b, and 2c).

Surfaces coated with noncharged bioinert layers of oligoethylene glycols (between three and six repeating units)

suppress protein adsorption and cell adhesion based on protein–protein interactions.<sup>27–30</sup> Such short oligomers, however, do not provide sufficient separation between the microspheres and the surfaces. Therefore, we focused on coatings composed of linear PEGs with MW of 1,000 Da and larger, i.e., polymers with more than 20 repeating units.

**Surface Derivatization and Characterization.** Using surface-chemistry protocols that we previously developed,<sup>15,31–34</sup> we coated glass slides with PEGs with MW = 1, 2, 3, 5, 10, and 20 kDa. Concurrently, resorting to carboxylated polymer microspheres (that were superparamagnetically doped) allowed us to PEGylate them via aqueous-phase coupling protocols. FTIR spectra confirmed the PEGylation of the superparamagnetically doped polymer beads. Furthermore, the beads manifested a positive shift in their  $\zeta$ -potentials after PEGylation, consistent with the loss of negative charges from the deprotonated free carboxyl groups. Electron microscopy showed that the PEGylation did not alter the morphology of the beads on micrometer and submicrometer scales (Figure 2a,b), which was consistent with the formation of

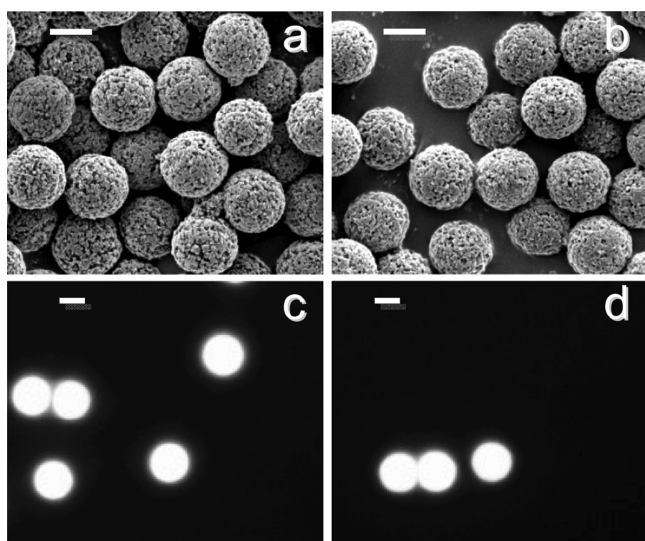


**Figure 2.** Images of superparamagnetically doped polymer beads (3- $\mu\text{m}$  diameter) used in this study. (a and b) Scanning-electron micrographs and (c and d) epifluorescence micrographs of beads that were (a and c) not coated and (b and d) coated with PEG-3000. For the electron microscopy images, the beads were coated with platinum. The autofluorescence of the beads was used for the fluorescence imaging. The scale bars correspond to 2  $\mu\text{m}$ .

passivation layers with thicknesses that did not exceed a few tens of nanometers.

Spectroscopic ellipsometry revealed that the thickness of the coatings did not increase proportionally with the length of the PEG chains (Table 1). Furthermore, the extent of drying had a pronounced effect on the measured thickness of the PEG layers.

For each sample, we observed two “metastable” states of PEG hydration when the polymer films were left in contact with air. (The ellipsometry studies were carried out in a clean-room environment with humidity maintained at 45%.) Draining the Milli Q water from the sample surfaces and letting them vent in the air led to constant thicknesses (within 30 min of drying) as monitored by ellipsometry ( $h_{\text{wet}}$  in Table 1). The water molecules bound to the PEG chains remained in these

“wet” films, making  $h_{\text{wet}}$  representative of the PEGylated surfaces when immersed in aqueous media.

Vigorous mechanical drying of the same samples (using a stream of dry nitrogen) decreased the thicknesses of the films (Table 1). Removal of most of the PEG-bound water appeared to have allowed the polymer chains to collapse and the films to thin. Although it is impossible to obtain complete dehydration of the PEG coatings under the conditions of the environment, the thicknesses of these “dry” films,  $h_{\text{dry}}$ , provided a handle for estimating the surface packing,  $\gamma$ , and the average distance,  $s$ , between the grafting sites (Table 1). Indeed, employing a materials model encompassing the parameters of pure PEG, provided excellent data fits for the ellipsometry spectra of the “dry” samples. In comparison, for the analysis of the “wet” samples, the data fits had higher  $\chi^2$  values than the  $\chi^2$  for the “dry” samples. As an alternative, we also allowed some of the optical parameters of the pure PEG film to relax in order to improve the fits.

For PEG-1000 the method of drying did not have a considerable effect on the coating thickness (Table 1). For the longer PEGs, while  $h_{\text{wet}}$  dropped when the PEG MW exceeded 10 kDa,  $h_{\text{dry}}$  manifested a trend of an increase with the PEG MW (Table 1). For all PEG MWs, the polymer Flory radii,  $R_F$ , were larger than the separation,  $s$ , between their grafting sites (Table 1). This finding ( $s < R_F < h_{\text{wet}}$ ) suggested that the PEGs in these coatings most probably existed as “brush” conformers.<sup>6,19</sup>

**Role of PEG Length.** Long-range interfacial interactions (eqs 1 and 2) provide key guidelines for the thicknesses of the passivation layers. Maintaining the interfacial interaction energies at levels that are comparable with the thermal energy,  $k_B T$ , requires inert layers that keep interfacial separation of tens of nanometers between the polymer microspheres and the flat glass surface.

To examine this somewhat oversimplified view on suppressing interfacial nonspecific interactions, we tested the dependence of the adhesion on the length of the PEGs composing the coatings on the beads and on the flat surfaces. When the microspheres and the glass substrates were coated with PEG-1000, on average about 60% of the beads remained on the surface upon applying 1.2-pN force (Figure 3a). An increase in the PEG length to about PEG-5000 led to a drastic decrease in the number of beads remaining adhered to the glass substrate in the presence of the pulling magnetic force (Figure 3a). Indeed, when the microspheres and the glass were coated with PEG-5000, only about 3% of the beads remained on the surface upon applying the magnetic pulling force.

An increase in the molecular weight of the coating PEGs to 10 kDa and 20 kDa led to an opposite trend. The number of remaining adhered beads increased with the increase in the PEG molecular weight (Figure 3a). This finding illustrated the limits in applying models for interactions between rigid substrates (eqs 1 and 2) to the mechanics of soft materials,<sup>35,36</sup> i.e., to surface coatings composed of flexible polymers.

Overall, films of linear PEGs with MW between 3 kDa and 10 kDa appeared optimal for suppressing adhesion between the microspheres and the glass surfaces. That is, for  $3 \text{ kDa} \leq \text{MW} \leq 10 \text{ kDa}$ , less than 1/5th of the beads remained adhered to the surface after applying piconewton pulling force (Figure 3a).

**Role of PEG Coatings.** PEG-3000 was the shortest polymer that provided acceptable suppression of nonspecific interfacial interactions between the microbeads and the flat substrate. Therefore, we employed PEG-3000 not only for

**Table 1. Properties of Surface Coatings of PEG with Different Molecular Weight (MW)**

MW <sub>PEG</sub> /Da	$h_{\text{dry}}/\text{nm}^a$	$\gamma/\text{nm}^{-2b}$	$R_F/\text{nm}^c$	$s/\text{nm}^d$	$h_{\text{wet}}/\text{nm}^e$	% beads <sup>f</sup>
1000	4.00 ± 0.01	2.65 ± 0.01	0.91	0.693 ± 0.004	4.00 ± 0.01	58.7 ± 61.0
2000	6.07 ± 0.02	2.01 ± 0.01	1.29	0.796 ± 0.004	10.1 ± 0.34	28.4 ± 38.2
3000	7.05 ± 0.94	1.56 ± 0.21	1.59	0.895 ± 0.093	16.3 ± 0.07	13.7 ± 5.8
5000	11.7 ± 0.4	1.55 ± 0.05	2.08	0.906 ± 0.022	22.8 ± 0.61	2.72 ± 0.68
10 000	10.2 ± 0.4	0.675 ± 0.026	3.04	1.37 ± 0.02	33.1 ± 0.03	8.1 ± 6.1
20 000	15.4 ± 0.5	0.510 ± 0.017	4.58	1.58 ± 0.01	26.8 ± 0.94	21.5 ± 4.2

<sup>a</sup>Average thickness of PEG coatings blown-dried with a stream of dry N<sub>2</sub> ( $h_{\text{dry}}$ ), obtained from spectroscopic ellipsometry. <sup>b</sup>Surface packing density in PEG chains per nm<sup>2</sup>:  $\gamma = 10^{-21} N_A h_{\text{dry}} \rho_{\text{PEG}} / \text{MW}_{\text{PEG}}$ , where  $N_A$  is the Avogadro number,  $h_{\text{dry}}$  is in nm,  $\rho_{\text{PEG}} = 1.1 \text{ g mL}^{-1}$ , and  $\text{MW}_{\text{PEG}}$  is in Da. <sup>c</sup>Flory radius,  $R_F$ , was estimated from the unperturbed radius of gyration,  $R_g$ :  $R_F = \alpha R_g$ .  $R_g = l ( \text{MW}_{\text{PEG}} / 6 \text{MW}_{\text{EG}} )^{1/2}$ , where  $l$  is length of the polymer residue ( $l = 0.358 \text{ nm}$ , corresponding to the oxygen–oxygen distance in all antistaggered conformer of 1,2-diethoxyethane from gas-phase-optimized MO structures), and  $\text{MW}_{\text{EG}}$  is the molecular weight (44 Da). The intermolecular expansion factor,  $\alpha$ , for PEG in water was estimated from reported data on the dependence of  $\alpha$  on  $\text{MW}_{\text{PEG}}$  and on the absolute temperature,  $T$ :  $\alpha \approx -1.3 + 8.8 \times 10^{-6} \text{ MW}_{\text{PEG}} + 760 / T$ .<sup>59</sup> <sup>d</sup>Average separation between the sites covalently holding the PEG chains to the surface:  $s = (4/\pi \gamma)^{1/2}$ .<sup>60</sup> <sup>e</sup>Average thickness of air-dried PEG coatings ( $h_{\text{wet}}$ ) in a class-1000 cleanroom (45% humidity level), obtained from spectroscopic ellipsometry. <sup>f</sup>Percent of beads remaining on the glass surface upon applying 1.2 pN pulling force for 5 s. The beads and the surfaces were coated with PEGs with the same MW.

investigating the interactions between PEGylated and bare surfaces, but also for analyzing the dependence of the adhesion on surfactant additives.

Coating the glass surfaces and the beads with PEG-3000 provided the means for suppressing nonspecific interactions (Tables 1 and 2). In contrast, when only the glass surfaces were coated with PEG-3000 and the beads were not coated, about 82% of the beads remained adhered after applying the magnetic force (Table 2). Similarly, when the glass was not coated and the beads were PEGylated, about 72% of the beads remained adhered after applying the pulling force (Table 2). These results show the importance of having both coated beads and coated glass surfaces for effective suppression of nonspecific interactions when using PEG-3000 for passivation.

Separating the microbeads from the glass surface with two PEG-3000 layers (each about 16-nm thick) provides a means to keep sufficient distance between polymer and the glass surfaces, which is essential for minimizing the interfacial interactions. Overlap between the PEG films induces repulsive forces essential for keeping the two substrates apart.<sup>35,37</sup> In contrast, the presence of only one PEG-3000 layer cannot provide wide enough separation between the substrates. It is consistent with the observed elevated adhesion when either only the beads or only the surfaces were PEGylated (Table 2).

As an alternative, identically prepared coatings of PEG-1000 and PEG-2000, had thicknesses of 4.0 and 10 nm, respectively. Coating the glass and the beads with these relatively thin PEG films did not sufficiently suppress the adhesion of the microspheres to the surfaces, as made evident by the copious amount of beads remaining on the glass upon applying 1.2-pN force (Table 1).

**Role of Noncharged Surfactant.** Despite the encouraging results, PEG-3000 coatings still did not provide quantitative suppression of the nonspecific adhesion, i.e., even when both substrates were PEGylated about 10–15% of the beads remained adhered to the surface after applying the magnetic forces. Defects in the PEG coatings are a plausible cause of the observed residual adhesiveness. Physisorption of PEG conjugates to coat the defects in the surface layers is a feasible venue for further suppression of the nonspecific interactions. The hydrophilic components of the TWEEN surfactants are composed of PEG chains. Therefore, we chose to use TWEEN in order to enhance the suppression of the adhesiveness of the interfaces.

To examine the effect of a noncharged surfactant on the adhesion between the beads and the glass surfaces, we added 10, 100, and 250  $\mu\text{M}$  of TWEEN20 to the microbead aqueous suspension prior to dropping it over the glass surfaces. The presence of 10  $\mu\text{M}$  TWEEN (that is under its CMC) had no detectable effect on suppressing the nonspecific adhesion. For most of the investigated interfaces, the adhesion-suppressing effect of the surfactant became apparent when its concentration increased to 250  $\mu\text{M}$  (Figure 4 and Table 2).

**Electrostatic Interactions.** In addition to the van der Waals interactions (along with the steric and the thermal-fluctuation and hydration interaction between the PEG layers leading to the entropic repulsion), the Coulombic interactions present another principal contributor to the nonspecific forces.<sup>5</sup> Therefore, it is essential to consider the charged groups on the different substrates when submerged in the neutral-pH aqueous media: (1) the noncoated glass surfaces were negatively charged, (2) the noncoated polymer beads were also negatively charged due to their derivatization with carboxylates, (3) PEG-coated glass surfaces may possess residual positive charges buried in the PEG layers close to the glass surface because the PEG chains were grafted to aldehyde-functionalized glass via reductive amination leaving secondary amines at the PEG-glass interface,<sup>15</sup> and (4) PEG-coated beads may possess residual negative charges due to nonreacted carboxylates (remaining buried under the PEG layers) after grafting the amine terminated PEGs to the carboxyl-functionalized beads via amide coupling. In addition, we prepared aminated glass slides for attaining a substrate with positively charged surfaces in which the charged groups were not buried under PEG coatings.

Noncoated beads with aminated glass surfaces provided attractive electrostatic interactions that were primarily derived from the negative charges from the deprotonated carboxyl groups on the beads and the positive charges from the protonated amines on the glass. In this experimental scenario, about 99% of the beads remained on the glass surface upon applying 1.2-pN force for five seconds. In contrast, noncoated beads and noncoated glass surfaces provided repulsive electrostatic interactions (where both surfaces were negatively charged), and only about 2% of the beads remained on the surface after the application of the magnetic force (Table 2).

Strictly speaking, the interaction energies, which govern the observed repulsion and adhesion between charged interfaces, are entropic in nature. In aqueous solutions, the electrostatic interactions fall off with distance quite substantially beyond a

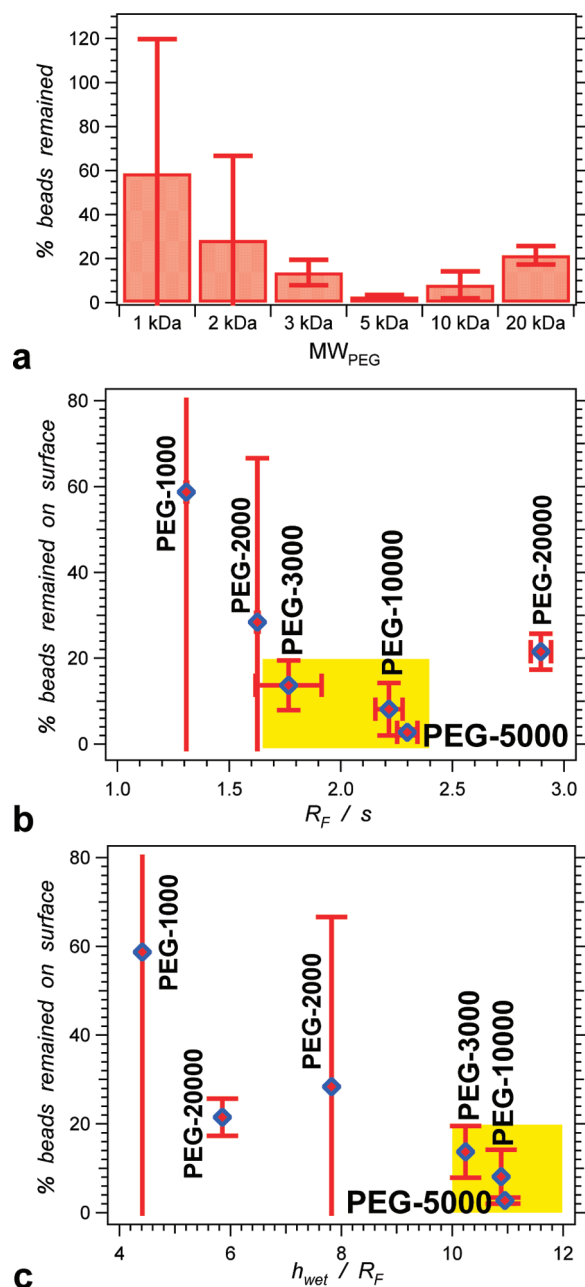


**Figure 3.** Adhesion between PEGylated superparamagnetically polystyrene microbeads (3- $\mu\text{m}$  diameter) and PEGylated glass surfaces (in an aqueous solution, with 100 mM phosphate buffer, pH 7). Adhesion is expressed as % beads remaining on the surfaces after 1.2 pN pulling force for about 5 s. (a) Category plot representing the dependence of the adhesion on the molecular weight of the PEG,  $MW_{\text{PEG}}$ , used for coating the beads and the surfaces. (b) Dependence of the adhesion on the ratio between the PEG Flory radius and the average distances between the grafting sites,  $R_F/s$ . (c) Dependence of the adhesion on the ratio between the layer thickness and the PEG Flory radius,  $h_{\text{wet}}/R_F$ .

few nanometers. In fact, the Debye length in the aqueous media we used (containing 100 mM phosphate buffer, pH 7) was about 6.5 Å, making the Coulombic forces significant only when the charged surfaces were practically in contact with one another. When the charged interfaces approached each other, the counterions were either (1) forced to bind to the charged sites (if the two surfaces had the same charge) leading to a

decrease in entropy (i.e., an unfavorable energy change resulting in repulsive force) or (2) expelled into the bulk solution (if the two surfaces were oppositely charged) leading to an entropy increase (i.e., a favorable energy change resulting in attractive force).

## DISCUSSION

While considering van der Waals interfacial interactions between micrometer-sized objects provided the initial guidelines for selecting the thickness of the surface coatings that suppress nonspecific adhesion, such an oversimplified view of the integrated dipole and induced-dipole interactions between two dielectric materials separated by aqueous media could not encompass the complexity of nonspecific attractive forces.<sup>5,38</sup> The surface of the polymer beads, for example, was not smooth and homogeneous (Figure 2a,b), and the van der Waals analysis did not take into consideration the molecular composition of the interfaces.

For PEG-1000 and PEG-2000, the enormous error bars from the adhesion measurements (Table 1) reflected the pronounced local variations in the morphologies of coated surfaces, i.e., they were indicative of the heterogeneity in the coatings. While ellipsometry averaged over the relatively large beam-reflection area used for the measurements (about 1 mm<sup>2</sup>), the pulling experiments probed the surfaces at contact areas that were considerably smaller than a square micrometer. Therefore, the discrepancies observed in the pulling measurements with PEG-1000 and PEG-2000 most probably were a corollary of the inability of the relatively short chains of these polymers to efficiently cover neighboring “pinhole” areas of exposed substrate surfaces that were not PEGylated at sufficient grafting densities.

Too well packed or too loosely packed PEG layers cannot suppress nonspecific adsorption and adhesion.<sup>39–41</sup> Indeed, the dense packing of PEG layers, containing PEGs in all-trans rather than helical conformation,<sup>39,42</sup> may offer an alternative explanation for the observed inefficient suppression of adhesion by the shortest PEG. Such all-trans PEG conformers, however, require packing densities of about 5 molecules per nm<sup>2</sup> (or more), corresponding to  $s < 0.5$  nm.<sup>39</sup> None of the surface coatings we investigated had such a high packing density, i.e., for all of them  $\gamma \leq 2.7$  nm<sup>-2</sup> and  $s \geq 0.7$  nm (Table 1). Therefore, excessively high density of packing with PEG-1000 and PEG-2000 did not contribute to their inefficiency in suppressing nonspecific adhesion.

For all coatings,  $s < R_F$ , suggesting that they were composed of PEGs in “brush” rather than in “mushroom” morphology.<sup>6,19</sup> While the increment per residue for all-trans PEG chains is about 0.36 nm, the increment per residue for PEG helical conformers (composing “brush” coatings) is about 0.28 nm.<sup>39</sup> Thus, to ensure helical conformation essential for “brush” morphology, the thickness of a film composed of PEG chains of  $N$  residues cannot exceed  $0.28N$  nm. For all the coatings we investigated, indeed,  $h_{\text{wet}} < 0.28N$  nm.

An increase in the packing density provides a means for forcing the helical conformers in the “brush” polymer layer to extend away from the surface and increase interfacial separation between coated substrates,<sup>43</sup> i.e.,  $R_F < h_{\text{wet}}$ . For suppressing adhesion, therefore, the PEGs have to be packed densely but not too densely.

How dense is dense? Considering the ratio between  $h_{\text{wet}}$  and  $R_F$  as a characteristic of packing-induced steric constraint of the polymer chains, allowed for setting apart the PEGs that

**Table 2.** Percent Paramagnetically Doped Polymer Microbeads Remaining Adhered on Glass Surfaces after Applying 1.2-pN Net Force for 5 s, in the Presence of Various Amount of TWEEN20<sup>a</sup>

TWEEN20 conc ( $\mu\text{M}$ )	PEG-coated glass surfaces <sup>b</sup>		noncoated glass surfaces		aminated glass surfaces <sup>c</sup>
	PEG-coated beads <sup>b</sup>	noncoated beads	PEG-coated beads <sup>b</sup>	noncoated beads	noncoated beads
0	13.7 $\pm$ 5.8	82.3 $\pm$ 9.1	72.3 $\pm$ 22.1	2.2 $\pm$ 0.6	98.7 $\pm$ 0.6
10	11.7 $\pm$ 2.6	85.2 $\pm$ 2.0	82.5 $\pm$ 21.6	4.6 $\pm$ 2.1	94.6 $\pm$ 2.6
100	7.6 $\pm$ 2.7	84.7 $\pm$ 5.4	89.7 $\pm$ 1.6	1.6 $\pm$ 0.8	95.2 $\pm$ 4.6
250	7.2 $\pm$ 1.9	14.9 $\pm$ 1.1	71.4 $\pm$ 12.5	0.2 $\pm$ 0.1	42.7 $\pm$ 1.3

<sup>a</sup>The beads (3- $\mu\text{m}$  diameter) were suspended in 100 mM aqueous phosphate buffer pH 7, with the indicated concentrations of surfactant, and allowed to settle on the glass surfaces for  $\sim 60$  s under gravity ( $0.3 \pm 0.1$  pN per bead), prior to applying the magnetic force. For each test the percentage of adhered beads was calculated from ratios between the count of the beads that were in focus at 5 s after applying the pulling force and immediately before applying the force. <sup>b</sup>Coated with PEG-3000. <sup>c</sup>Amine-coated via treatment with 4-butylammoniumtriethoxysilane.

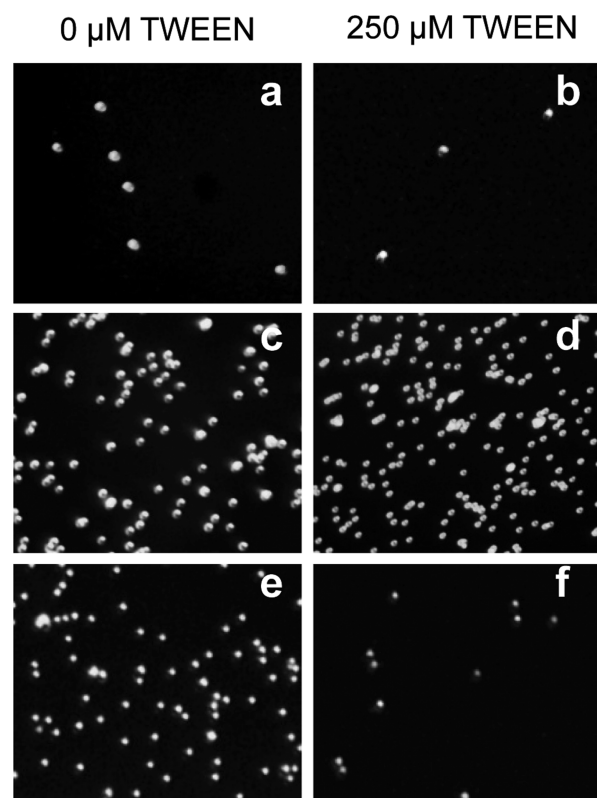


**Figure 4.** Reflection microscopy images of beads remaining on flat glass surfaces after applying 1.2-pN force for 5 s: (a, c, and e) in the absence of surfactant; and (b, d, and f) in the presence of 250  $\mu\text{M}$  TWEEN20. (a and b) PEG-coated beads on PEG-coated surfaces; (c and d) PEG-coated beads on noncoated surfaces; and (e and f) noncoated beads on PEG-coated surfaces. The coatings were of PEG-3000. The beads were suspended in 100 mM aqueous phosphate buffer, pH 7, in the presence or absence of surfactant as indicated, and allowed to settle for  $\sim 3$  min prior to applying the pulling magnetic force.

provided optimal adhesion suppression, i.e., for PEG-3000, PEG-5000, and PEG-10000,  $h_{\text{wet}}/R_{\text{F}} > 10$  (Figure 3c). The decrease in  $h_{\text{wet}}/R_{\text{F}}$  as the PEG MW increased from 5 kDa to 20 kDa was consistent with the observed decrease in the efficiency of adhesion suppression (Figure 3c). While maintaining  $s > 0.52$  nm and  $h < 0.28$  nm,<sup>39</sup> attaining  $h_{\text{wet}}/R_{\text{F}} > 10$  could serve as a guideline for PEG coatings that suppress undesired adhesion between micrometer-size objects.

Addition of TWEEN20 suppressed the attractive interactions between oppositely charged surfaces only when the surfactant was used in excessive concentrations, i.e., 0.25 mM (Table 2). A

plausible explanation of the observed results is that the physisorption of the surfactant on the substrate surface led to the suppression of the electrostatic interactions by burying the charged groups and changing the structure of the double layers. Therefore, charged groups coated by the PEG layers were not expected to contribute significantly to the observed nonspecific interactions. Furthermore, the counterions of such buried charged groups would be immobilized in the PEG layers, making the behavior of such trapped ion pairs closer to the behavior of dipoles than to that of individual charges.

Our findings demonstrated a dependence of the efficacy of decreasing the extent of nonspecific interfacial interactions on the surfactant concentration. The results, however, revealed that complications arise if only surfactants were employed for the suppression of nonspecific interactions. Since surfactants are required in considerably high concentrations, they would be capable of disrupting not only biomolecular tertiary and quaternary structures, but also sensitive electrostatic and other biospecific interactions as seen with the noncoated beads on aminated surfaces.

Are TWEEN surfactants needed for suppressing nonspecific interactions? As moderate surfactants, the different TWEEN conjugates are widely used in biology and in biophysics, including for suppressing nonspecific adhesion.<sup>10–12,28</sup> Our findings, however, do not provide convincing evidence for the benefit of TWEEN in suppressing nonspecific interfacial interactions. Although addition of TWEEN20 decreased the amount of the nonspecifically adhered microbeads by a factor of 2, the concentrations of the used surfactant were high enough to considerably perturb the properties of investigated biological systems, making the use of such surfactant unfeasible for SMFMs.

Why PEG? PEG is an amphipathic polymer that intercalates well in the water structure, and hence does not significantly perturb the three-dimensional molecular composition of the media.<sup>44</sup> The distances between the oxygens in a PEG chain match well with the hydrogen-bonding network of water, providing the means for stable hydration shells around the hydrophobic stretches of the polymer (i.e., around the ethylenes). Thus, the PEG chains form networks supporting the water structure (e.g., hydrogels) and do not interact with one another (or with other macromolecules) at temperatures and pressures under which the polymer hydration is intact. Therefore, PEG is biocompatible and coatings of PEG (in brush conformation) prevent adsorption of biological macromolecules.<sup>15,28,45–47</sup> While PEG is not necessarily unique and other materials are also potentially biocompatible and suppress nonspecific adsorption,<sup>29,48,49</sup> the biophysics of PEG has been extensively investigated and its chemistry well developed to

allow broad versatility for the preparation of robust bioinert and biofunctional interfaces.<sup>15,50,51</sup> Overall, the PEGylation of the surfaces serves two main functions: (1) it creates a separation between the two surfaces and (2) it introduces entropic repulsion between the surfaces,<sup>52</sup> as it is not energetically favorable to compress the PEG strands between the approaching interfaces when the hydrated polymer chains are in their brush conformation.<sup>50,53–55</sup>

## CONCLUSIONS

The functionality of biological molecules does not get compromised upon covalent attachment to PEG bioinert layers.<sup>15</sup> This consideration, along with the ability of PEG coatings to suppress nonspecific interfacial interactions, will prove immensely important and beneficial for SMFMs. Because there are more disadvantages than benefits to using TWEEN for suppressing undesired adhesion, we believe that the emphasis should be on improving nonadhesiveness via a rational design of surface coatings, rather than on taking “short-cuts” by using surfactants and other additives. Employing surfactants in SMFM studies, indeed, undermines the ability to study proteins with native functionality.

Nevertheless, an examination of the molecular structures of the TWEEN surfactants revealed that the use of coatings of branched PEG derivatives might provide further suppression of nonspecific interactions. (The PEG chains in the TWEENS are branched out of a sorbitan.) Such venues for rational interfacial design at multiscale levels (from molecular to micrometer dimensions) are crucial for advancing the tools for SMFMs.

For linear PEG chains, however, we observed that the ratio between the film thickness and the Flory radius of the polymers composing the film correlated excellently with the ability of these PEG coatings to suppress undesired adhesion. Testing this correlation in as many different applications as possible will provide the means to examine the potential universality and the limits in using the thickness-to-radius ratio for predicting resistance against nonspecific interfacial interactions.

## EXPERIMENTAL SECTION

**Materials.** Polymer microspheres, ProMag, superparamagnetically doped with magnetite (that have carboxyl functional groups, with a mean diameter of 3  $\mu\text{m}$  and 1.9  $\text{g}/\text{cm}^3$  density) were purchased from Bangs Laboratories, Inc., in January 2009. Precleaned 1 mm thick microscope glass slides were purchased from VWR and cut into 25  $\times$  35 mm pieces prior to use. Silicon wafers (n/phosphorus and p/boron doped, 1–10  $\Omega$  cm, one side polished, test grade,  $\langle 100 \rangle$ ) were purchased from Silicon Sense, Inc., and cut into 25  $\times$  10 mm prior to use.

The polymers,  $\alpha,\omega$ -aminomethoxy polyethylene glycol (MeO-PEG-NH<sub>2</sub>), MW = 1, 2, 3, 5, 10, and 20 kDa, were purchased from Layson Bio. 11-Aminoundecyltriethoxysilane and 11-(triethoxysilyl)undecanaldehyde acetal were purchased from Gelest, Inc. Indium(III) chloride (99.999%), redistilled *N,N*-diisopropylethylamine (DIPEA), TWEEN20 surfactant, and sodium cyanoborohydride were purchased from Aldrich. *N,N*-Diisopropylcarbodiimide (DIC) and *N*-hydroxysuccinimide (HOSu) were obtained from Lancaster. Hydroxybenzotriazole (HOBt) was purchased from Chem-Impex International. 1-Ethyl-3-(3-dimethylaminopropyl) carbodiimide (EDC), toluene, tetrahydrofuran (THF), methanol, and ethanol, all spectroscopy grade and/or anhydrous, were obtained from Fisher.

**Coating and Characterization of Flat Substrates.** Using a surface chemistry protocol that we previously developed,<sup>15</sup> we functionalized glass slides with varying lengths of MeO-PEG-NH<sub>2</sub>. For ellipsometry measurements, we prepared identical coatings on

silicon wafers.<sup>15</sup> We monitored the completion of PEGylation reaction via surface contact angle measurements.<sup>31</sup>

For the aminated control surfaces, we salinized glass slides with alkyleneamines by (1) cleaning them as we previously described,<sup>15</sup> (2) treating them with oxygen plasma,<sup>31,32</sup> and (3) immersing them in an anhydrous toluene solution of 0.04% (v/v) of 11-aminoundecyltriethoxysilane and 0.02% DIPEA. The glass slides, immersed in the salinization solution, were heated on a sand bath at 110  $^{\circ}\text{C}$ , and were sonicated in hot water intermittently for 60 s after the first hour. After 18 h, the salinization bath was allowed to cool to room temperature, the solution was discarded, and the glass slides were doubly washed with toluene, dichloromethane, THF, ethanol, and deionized/milli Q water.

**Coating and Characterization of Microbeads.** The PEGylation of the beads involved the following principal steps.

**Cleaning.** Ten  $\mu\text{L}$  of a suspension of magnetic beads were placed in a 1 mL microfuge tube containing 250  $\mu\text{L}$  solution of 0.01 M sodium hydroxide (NaOH), and gently shaken at room temperature for 10 min. The beads were trapped with a permanent magnet at the bottom of the tube for 5 min and the solution was decanted. This wash step was repeated twice. 500  $\mu\text{L}$  of deionized water was then added to the centrifuge tube and gently shaken at room temperature for 5 min. The water-bead solution was decanted and the process repeated three times.

**PEG Coupling.** In a cold room, the water was removed from the centrifuge tube, and 200  $\mu\text{L}$  solutions of HOSu and EDC were added to the beads, followed by addition of MeO-PEG-NH<sub>2</sub>. The solution was gently shaken in the cold room (4  $^{\circ}\text{C}$ ). After overnight shaking, the solution was brought back to room temperature for 2–4 h and washed with plenty of deionized water and decanted. Beads were stored in deionized water at 2–8  $^{\circ}\text{C}$  until needed.

**Verification.** The presence of the PEG coatings was confirmed using FTIR as we have previously demonstrated.<sup>40</sup> The completion of the coupling reaction was monitored by measuring the  $\zeta$ -potential of the beads. The covalent modification of the polymer beads with PEG led to a positive shift in the  $\zeta$ -potentials, resultant from the elimination of the negatively charged carboxylic acid groups.

**Ellipsometry.** Spectra of the phase ( $\Delta$ ) and the amplitude ( $\Psi$ ) were recorded between 400 and 700 nm for three angles of incidence, 60 $^{\circ}$ , 70 $^{\circ}$ , and 80 $^{\circ}$ , using Horiba Jobin Yvon UVISSEL spectroscopic ellipsometer, model M200. The measurements were conducted in a class-1,000 clean room, with humidity maintained at 45 ( $\pm 1$ ) %. The samples were mounted on an ellipsometer stage exposed to air.

For the “wet” PEG coatings, the samples (coated silicon wafers stored under water) were washed with Milli-Q water and kept vertically to dry over dust-free wiper tissue for at least half an hour prior to the measurements. For the ellipsometry spectra of the “dry” coatings, the PEGylated surfaces of the same samples were blown with copious amounts of dry nitrogen for at least 5 min.

The thicknesses of the PEG layers,  $h_{\text{dry}}$  and  $h_{\text{wet}}$  (Table 1), were obtained from global fits of the ellipsometry spectra recorded at the different angles. A two-layer model, air//PEG/SiO<sub>2</sub>/Si,<sup>15</sup> provided excellent fits for the spectra of all samples. Using models based on a single layer or on more than two layers did not yield satisfactory data fits. The fitting algorithm minimized the  $\chi^2$  values and the fitting residuals revealed the goodness of the fits. The thickness of the SiO<sub>2</sub> layer was about 2.2 nm and the thickness of the PEG layer varied with the MW of the polymer (Table 1).

Established parameters for all materials were incorporated in the data analysis software, DeltaPsi v2.4.3.158 (Horiba Jobin Yvon, Inc.). For the PEG material layer in the fitting model, we used the default parameters provided by the Thin Film Division at HORIBA Jobin Yvon, Inc.,  $\epsilon_{\infty} = 1.0$ ,  $\epsilon_s = 1.633$ ,  $\omega_1 = 9.723$ , and  $\Gamma_0 = 4.921$ .<sup>56</sup> For this study, we used the layer thicknesses obtained from data fits for which these parameters were fixed. Relaxing these parameters for the analyses of the “dry” samples did not improve the quality of the fits, and produced negative values for some of the dielectric quantities. Relaxing the parameters for the “wet” samples resulted in a slight improvement of the quality of the fits, and, within physically feasible values of the quantities characteristic of the PEG material, yielded layer thicknesses

of 2.7, 9.1, 22, 35, and 27 nm for PEGs with MW 1, 2, 3, 5, 10, and 20 kDa, respectively. Nevertheless, because we did not have a basis for judging the plausibility in the variations of the fitting dielectric and optical parameters, we used the results from the data fits with fixed parameters (i.e., using a model for pure PEG for analyzing the data from the wet PEG samples) with the understanding that the values of  $h_{\text{wet}}$  reported in Table 1, might be underestimated.

**Microscopy.** Fluorescence microscopy images were acquired using a Nikon Ti-U inverted microscope (Nikon, Inc., Melville, NY), equipped with a 100× Nikon oil immersion objective (numerical aperture, 1.49; working distance, 120 μm) and a Hamamatsu electron multiplier charge-coupled-device digital camera (model C9100-13; Hamamatsu Corp., Bridgewater, NJ), as we previously described.<sup>57</sup> Suspension of superparamagnetic beads was dropped on a glass slide, placed over the objective of the microscope, and the beads were allowed to settle on the glass surface. Using bright-field mode, the objective was focused on the settled beads, and for the imaging, it was turned into fluorescence mode utilizing the autofluorescence from the polymer material composing the microspheres ( $\lambda_{\text{em}} = 536$  nm, bandwidth = 25 nm).

Scanning electron microscopy images were recorded using FEI XL30-FEG SEM. Prior to imaging, the superparamagnetic beads were

**Table 3. Forces Measured at Different Horizontal Distances,  $x$ , from the Center of the Electromagnet and Different Vertical Distances,  $y$ , from the Tip of the Electromagnet (at 12 V)**

$y/\text{mm}$	$x/\text{mm}$		
	0.0	0.25	0.50
1.00	$1.8 \pm 0.4$	$1.7 \pm 0.5$	$2.0 \pm 0.4$
1.25	$1.4 \pm 0.2$	$1.3 \pm 0.3$	$1.7 \pm 0.4$
1.50	$1.5 \pm 0.3$	$1.2 \pm 0.5$	$1.3 \pm 0.5$
1.75	$1.3 \pm 0.1$	$1.4 \pm 0.04$	$1.4 \pm 0.03$

washed with Milli Q water several times, lyophilized, spread on a sample stage, and sputter-coated with a conductive layer (80% Pt and 20% Pd).

**Calibration of the Magnetic Puller.** We built a magnetic puller setup to carry out the adhesion studies (Scheme S1). We designed the setup in two interchangeable configurations: (1) “work mode” for measurements of the number of beads on a flat surface of a transparent substrate (Scheme 1a), in which the objective is positioned below the sample slide, and (2) “calibration mode” for force calibration (Scheme 2), in which the objective provides a side view of the suspension allowing for tracking the position of beads as they move vertically in response to the magnetic field. The two parameters used for controlling the force experienced by the paramagnetic beads are (1) the distance from the core of the electromagnet and (2) the current flowing through the coil of the electromagnet, controlled by the applied voltage.

Stoke’s drag equation allowed us to determine the forces generated on each super paramagnetic bead at different distances and different applied voltages (Figure 5)

$$F_d = -6\pi\mu r v \quad (3)$$

where  $F_d$  is the drag force,  $\mu$  is the dynamic viscosity of the media, and  $r$  is the radius of a bead that moves with velocity  $v$ . The viscosity of the solutions used for the force calibrations was measured using a Cannon-Fenske N 956 Size 150 viscometer.

Because the employed forces were relatively weak, we accounted for the gravitational pull on the suspended beads. The magnetic force that pulls the beads upward opposes the drag force and the gravitational force. Two different approaches allowed us to determine the gravitational force: (1) calculate it by accounting for the bead buoyancy using the Archimedes’ principle, from the density of the solution (measured with a Mettler Toledo portable density meter, Densito 30PX), and from the density and the volume of the beads and

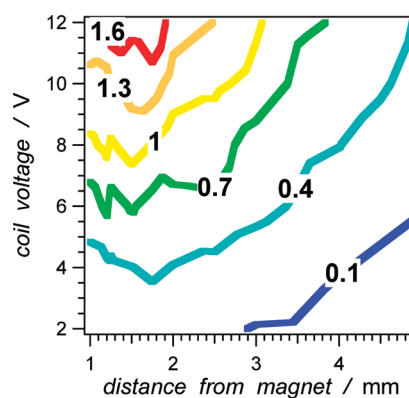


**Figure 5.** Dependence of the magnetic force,  $F_m$ , on the applied voltage and on the distance from the magnet tip, represented as a counter plot. ( $F_m$  is in pN.) The forces were extracted from the velocities of beads moving upward toward the center of the magnet (within a strip  $\pm 0.1$  mm from the central line, and maintaining constant velocity within  $\pm 0.1$  mm around the designated distance from the magnet). From the velocities, the drag forces,  $F_d$ , were calculated (eq 3). The difference between  $F_m$  and the gravitational force,  $F_g$ , opposes  $F_d$ , the magnitude of which, represents the net force,  $F_N$ , that each bead experiences:  $F_m = -F_d - F_g$  and  $F_N = F_m - F_g$ . Each data point is an average from the measured velocities of at least three to five beads.

(2) estimate it from the measured velocities with which the beads settle down. The former and the latter approach provided values for gravitational force of 0.1 pN and 0.3 pN, respectively, that each suspended bead experienced.

The dependence of the magnetic force on the horizontal distance from the magnet core and on the vertical distance from the center of the magnet was tested using a 2-factor ANOVA as implemented by Igor Pro (version 6.22A).<sup>58</sup> The side field of view of the bead suspension was separated into four vertical and three horizontal sections, and the velocities of beads in any of the 12 quadrants were measured. From the measured velocities, we calculated the magnetic forces exerted on the beads (Table 3). The two null hypotheses for the ANOVA test were that the magnetic pulling force did not depend on the horizontal position,  $x$ , and on the vertical position,  $y$ . The  $p$  values obtained from the 2-factor ANOVA were  $p_x = 0.44$ ,  $p_y = 0.030$ , and  $p_{xy} = 0.95$ , not allowing the rejection of the lack of dependence on  $x$ , but allowing the rejection of the lack of dependence on  $y$  (assuming  $\alpha = 0.05$ ). This finding indicated that all beads within the horizontal field of view (in work mode) experienced the same force.

**Measuring Desorption of Beads from Glass Surfaces.** For a typical adhesion experiment, we placed the calibrated electromagnet  $\sim 1.5$  mm from the surface of the glass (Scheme 1a) and applied 12 V to achieve 1.5 pN of magnetic force. Accounting for the opposing gravitational force provided an estimate of  $1.2 \pm 0.3$  pN for net force pulling upward, which each bead experienced when the magnet was turned on.

Using the magnetic puller in a work mode (Scheme 1a), we injected a suspension of beads into a PDMS well on the glass slide. By focusing the objective at the surface of the glass, we observed only the beads that settled on the surface, thereby disregarding the beads that had not made contact with the glass.

After allowing the beads to settle on the glass bottom of the well for 3 min, we turned on the electromagnet to exert a relatively weak net force ( $\sim 1.2$  pN) pulling upward, away from the glass surface. Using a CCD camera (at 10 frames per second), we recorded the beads on the surface from 3 to 5 s before the electromagnet was switched on, to 8–10 s after. The movies were saved as stacks of images and the number of beads remaining on the surface with respect to time was analyzed using Imaris Bitplane software.

## ■ AUTHOR INFORMATION

## Corresponding Author

\*Phone (951) 827-6239. Fax (951) 827-6416. E-mail vullev@ucr.edu; Webpage: <http://www.vullevgroup.ucr.edu>.

## Present Addresses

<sup>1</sup>Department of Clinical Laboratory Science, Loma Linda University, Loma Linda, CA 92350.

<sup>#</sup>Department of Bioengineering and the McGowan Institute for Regenerative Medicine, University of Pittsburgh, Pittsburgh, PA 15219.

<sup>∇</sup>Department of Bioengineering, University of California, Berkeley, CA 94720.

## Notes

The authors declare no competing financial interest.

## ■ ACKNOWLEDGMENTS

The U.S. National Science Foundation provided funding for this research (CBET 0935995 and EEC 0649096). Dr. Kishore Uppireddi from Thin Film Division at Horiba Jobin Yvon, Inc., provided assistance with the ellipsometry modeling and analysis. The electron-microscopy studies were conducted under the supervision of Dr. Krassimir N. Bozhilov at the Central Facility for Advanced Microscopy and Microanalysis at the University of California, Riverside, established with funding from the U.S. National Science Foundation. We also thank Mr. George Ibrahim, Ms. Katie Peterson, Mr. Andrew Vu, and Mr. Jyann-Tyng Lu for the initial design and the assembly of the magnetic-puller setup.

## ■ REFERENCES

- (1) Kapanidis, A. N.; Strick, T. Biology, one molecule at a time. *Trends Biochem. Sci.* **2009**, *34*, 234–243.
- (2) Neuman, K. C.; Nagy, A. Single-molecule force spectroscopy: optical tweezers, magnetic tweezers and atomic force microscopy. *Nat. Methods* **2008**, *5*, 491–505.
- (3) Ainavarapu, S. R. K.; Wiita, A. P.; Dougan, L.; Uggerud, E.; Fernandez, J. M. Single-molecule force spectroscopy measurements of bond elongation during a bimolecular reaction. *J. Am. Chem. Soc.* **2008**, *130*, 6479–6487.
- (4) Pum, D.; Horejs, C.; Ristl, R.; Tscheliessnig, R.; Sleytr, U. B. Single-molecule Force Spectroscopy Reveals the Individual Mechanical Unfolding Pathways of a Surface Layer Protein. *J. Biol. Chem.* **2011**, *286*, 27416–27424.
- (5) Israelachvili, J. Differences between non-specific and bio-specific, and between equilibrium and non-equilibrium, interactions in biological systems. *Q. Rev. Biophys.* **2005**, *38*, 331–337.
- (6) Leckband, D.; Israelachvili, J. Intermolecular forces in biology. *Q. Rev. Biophys.* **2001**, *34*, 105–267.
- (7) Hickman, J. J.; Sweryda-Krawiec, B.; Devaraj, H.; Jacob, G. A new interpretation of serum albumin surface passivation. *Langmuir* **2004**, *20*, 2054–2056.
- (8) Niedzwiecki, D. J.; Grazul, J.; Movileanu, L. Single-Molecule Observation of Protein Adsorption onto an Inorganic Surface. *J. Am. Chem. Soc.* **2010**, *132*, 10816–10822.
- (9) Schoenfish, M. H.; Brogan, K. L.; Shin, J. H. Influence of surfactants and antibody immobilization strategy on reducing nonspecific protein interactions for molecular recognition force microscopy. *Langmuir* **2004**, *20*, 9729–9735.
- (10) Zhang, W.; Ang, W. T.; Xue, C. Y.; Yang, K. L. Minimizing nonspecific protein adsorption in liquid crystal immunoassays by using surfactants. *ACS Appl. Mater. Interfaces* **2011**, *3*, 3496–3500.
- (11) Danilowicz, C.; Greenfield, D.; Prentiss, M. Dissociation of ligand-receptor complexes using magnetic tweezers. *Anal. Chem.* **2005**, *77*, 3023–3028.

(12) Wahlgren, M.; Welin-Klintström, S.; Arnebrant, T.; Askendal, A.; Elwing, H. Competition between fibrinogen and a non-ionic surfactant in adsorption to a wettability gradient surface. *Colloids Surf. B* **1995**, *4*, 23–31.

(13) Vullev, V. I.; Jones, G. Photoinduced electron transfer in alkanoylpyrene aggregates in conjugated polypeptides. *Tetrahedron Lett.* **2002**, *43*, 8611–8615.

(14) Otzen, D. Protein-surfactant interactions: A tale of many states. *Biochim. Biophys. Acta, Proteins Proteom.* **2011**, *1814*, 562–591.

(15) Wan, J.; Thomas, M. S.; Guthrie, S.; Vullev, V. I. Surface-bound proteins with preserved functionality. *Ann. Biomed. Eng.* **2009**, *37*, 1190–1205.

(16) Vullev, V. I.; Wan, J.; Heinrich, V.; Landsman, P.; Bower, P. E.; Xia, B.; Millare, B.; Jones, G. II Nonlithographic Fabrication of Microfluidic Devices. *J. Am. Chem. Soc.* **2006**, *128*, 16062–16072.

(17) Thomas, M. S.; Clift, J. M.; Millare, B.; Vullev, V. I. Print-and-Peel Fabricated Passive Micromixers. *Langmuir* **2010**, *26*, 2951–2957.

(18) Bijamov, A.; Shubitidze, F.; Oliver, P. M.; Vezenov, D. V. Quantitative modeling of forces in electromagnetic tweezers. *J. Appl. Phys.* **2010**, *108*, 104701/104701–104701/104709.

(19) Israelachvili, J. N. *Intermolecular and Surface Forces*, 2 ed.; Academic Press: New York, 1992.

(20) Vasquez, J. M.; Vu, A.; Schultz, J. S.; Vullev, V. I. Fluorescence enhancement of warfarin induced by interaction with beta -cyclodextrin. *Biotechnol. Prog.* **2009**, *25*, 906–914.

(21) Bard, A. J.; Faulkner, L. R. *Electrochemical Methods: Fundamentals and Applications*, 2nd ed.; Wiley: New York, 2001.

(22) Bao, D.; Ramu, S.; Contreras, A.; Upadhyayula, S.; Vasquez, J. M.; Beran, G.; Vullev, V. I. Electrochemical Reduction of Quinones: Interfacing Experiment and Theory for Defining Effective Radii of Redox Moieties. *J. Phys. Chem. B* **2010**, *114*, 14467–14479.

(23) Upadhyayula, S.; Bao, D.; Millare, B.; Sylvia, S. S.; Habib, K. M. M.; Ashraf, K.; Ferreira, A.; Bishop, S.; Bonderer, R.; Baqai, S.; Jing, X.; Penchev, M.; Ozkan, M.; Ozkan, C. S.; Lake, R. K.; Vullev, V. I. Permanent Electric Dipole Moments of Carboxyamides in Condensed Media: What Are the Limitations of Theory and Experiment? *J. Phys. Chem. B* **2011**, *115*, 9473–9490.

(24) Bao, D.; Millare, B.; Xia, W.; Steyer, B. G.; Gerasimenko, A. A.; Ferreira, A.; Contreras, A.; Vullev, V. I. Electrochemical Oxidation of Ferrocene: A Strong Dependence on the Concentration of the Supporting Electrolyte for Nonpolar Solvents. *J. Phys. Chem. A* **2009**, *113*, 1259–1267.

(25) Hu, J.; Xia, B.; Bao, D.; Ferreira, A.; Wan, J.; Jones, G.; Vullev, V. I. Long-Lived Photogenerated States of alpha-Oligothiophene-Acrindinium Dyads Have Triplet Character. *J. Phys. Chem. A* **2009**, *113*, 3096–3107.

(26) Israelachvili, J. N.; Ninham, B. W. Intermolecular forces - the long and short of it. *J. Colloid Interface Sci.* **1977**, *58*, 14–25.

(27) Mrksich, M.; Whitesides, G. M. Using self-assembled monolayers to understand the interactions of man-made surfaces with proteins and cells. *Annu. Rev. Biophys. Biomol. Struct.* **1996**, *25*, 55–78.

(28) Hu, K.; Gao, Y.; Zhou, W.; Lian, J.; Li, F.; Chen, Z. Fluorinated silicon surfaces under mixed surfactants: resistance to nonspecific protein adsorption for biosensing. *Langmuir* **2009**, *25*, 12404–12407.

(29) Chapman, R. G.; Ostuni, E.; Takayama, S.; Holmlin, R. E.; Yan, L.; Whitesides, G. M. Surveying for Surfaces that Resist the Adsorption of Proteins. *J. Am. Chem. Soc.* **2000**, *122*, 8303–8304.

(30) Chen, C. S.; Mrksich, M.; Huang, S.; Whitesides, G. M.; Ingber, D. E. Geometric control of cell life and death. *Science* **1997**, *276*, 1425–1428.

(31) Millare, B.; Thomas, M.; Ferreira, A.; Xu, H.; Holesinger, M.; Vullev, V. I. Dependence of the quality of adhesion between polydimethyl siloxane and glass surfaces on the conditions of treatment with oxygen plasma. *Langmuir* **2008**, *24*, 13218–13224.

(32) Chau, K.; Millare, B.; Lin, A.; Upadhyayula, S.; Nuñez, V.; Xu, H.; Vullev, V. I. Dependence of the quality of adhesion between poly(dimethylsiloxane) and glass surfaces on the composition of the oxidizing plasma. *Microfluid. Nanofluid.* **2011**, *10*, 907–917.

- (33) Hong, C.; Bao, D.; Thomas, M. S.; Clift, J. M.; Vullev, V. I. Print-and-Peel Fabrication of Microelectrodes. *Langmuir* **2008**, *24*, 8439–8442.
- (34) Thomas, M. S.; Millare, B.; Clift, J. M.; Bao, D.; Hong, C.; Vullev, V. I. Print-and-peel fabrication for microfluidics: what's in it for biomedical applications? *Ann. Biomed. Eng.* **2010**, *38*, 21–32.
- (35) Drobek, T.; Spencer, N. D.; Heuberger, M. Compressing PEG brushes. *Macromolecules* **2005**, *38*, 5254–5259.
- (36) Jones, G. I.; Yan, D.; Hu, J.; Wan, J.; Xia, B.; Vullev, V. I. Photoinduced Electron Transfer in Arylacridinium Conjugates in a Solid Glass Matrix. *J. Phys. Chem. B* **2007**, *111*, 6921–6929.
- (37) Kenworthy, A. K.; Hristova, K.; Needham, D.; McIntosh, T. J. Range and Magnitude of the Steric Pressure between Bilayers Containing Phospholipids with Covalently Attached Poly(Ethylene Glycol). *Biophys. J.* **1995**, *68*, 1921–1936.
- (38) Vullev, V. I. Modulation of dissociation kinetics by external force: examination of the Bell model. *J. Biol. Sci.* **2005**, *5*, 744–758.
- (39) Harder, P.; Grunze, M.; Dahint, R.; Whitesides, G. M.; Laibinis, P. E. Molecular Conformation in Oligo(ethylene glycol)-Terminated Self-Assembled Monolayers on Gold and Silver Surfaces Determines Their Ability To Resist Protein Adsorption. *J. Phys. Chem. B* **1998**, *102*, 426–436.
- (40) Bahmani, B.; Gupta, S.; Upadhyayula, S.; Vullev, V. I.; Anvari, B. Effect of polyethylene glycol coatings on uptake of indocyanine green loaded nanocapsules by human spleen macrophages in vitro. *J. Biomed. Opt.* **2011**, *16*, 051303/051301–051303/051310.
- (41) Majewski, J.; Kuhl, T. L.; Kjaer, K.; Gerstenberg, M. C.; Als-Nielsen, J.; Israelachvili, J. N.; Smith, G. S. X-ray Synchrotron Study of Packing and Protrusions of Polymer-Lipid Monolayers at the Air-Water Interface. *J. Am. Chem. Soc.* **1998**, *120*, 1469–1473.
- (42) Feldman, K.; Hähner, G.; Spencer, N. D.; Harder, P.; Grunze, M. Probing resistance to protein adsorption of oligo(ethylene glycol)-terminated self-assembled monolayers by scanning force microscopy. *J. Am. Chem. Soc.* **1999**, *121*, 10134–10141.
- (43) Heuberger, M.; Drobek, T.; Spencer, N. D. Interaction forces and morphology of a protein-resistant poly(ethylene glycol) layer. *Biophys. J.* **2005**, *88*, 495–504.
- (44) Israelachvili, J. The different faces of poly(ethylene glycol). *Proc. Natl. Acad. Sci. U.S.A.* **1997**, *94*, 8378–8379.
- (45) Janshoff, A.; Neitzert, M.; Oberdorfer, Y.; Fuchs, H. Force Spectroscopy of Molecular Systems-Single Molecule Spectroscopy of Polymers and Biomolecules. *Angew. Chem., Int. Ed. Engl.* **2000**, *39*, 3212–3237.
- (46) Shang, H.; Lee, G. U. Magnetic tweezers measurement of the bond lifetime-force behavior of the IgG-protein A specific molecular interaction. *J. Am. Chem. Soc.* **2007**, *129*, 6640–6646.
- (47) Joo, C.; Balci, H.; Ishitsuka, Y.; Buranachai, C.; Ha, T. Advances in single-molecule fluorescence methods for molecular biology. *Annu. Rev. Biochem.* **2008**, *77*, 51–76.
- (48) Deng, L.; Mirksich, M.; Whitesides, G. M. Self-Assembled Monolayers of Alkanethiolates Presenting Tris(propylene sulfoxide) Groups Resist the Adsorption of Protein. *J. Am. Chem. Soc.* **1996**, *118*, 5136–5137.
- (49) Chen, S. F.; Zheng, J.; Li, L. Y.; Jiang, S. Y. Strong resistance of phosphorylcholine self-assembled monolayers to protein adsorption: Insights into nonfouling properties of zwitterionic materials. *J. Am. Chem. Soc.* **2005**, *127*, 14473–14478.
- (50) Yu, H. U.; Yang, Z. H.; Galloway, J. A. Protein interactions with poly(ethylene glycol) self-assembled monolayers on glass substrates: Diffusion and adsorption. *Langmuir* **1999**, *15*, 8405–8411.
- (51) Harris, J. M. *Poly(ethylene glycol) chemistry: biotechnical and biomedical applications*; Plenum Press: New York, 1992.
- (52) Israelachvili, J. N.; Wennerstroem, H. Entropic forces between amphiphilic surfaces in liquids. *J. Phys. Chem.* **1992**, *96*, 520–531.
- (53) Bergstrom, K.; Holmberg, K.; Safranj, A.; Hoffman, A. S.; Edgell, M. J.; Kozlowski, A.; Hovanes, B. A.; Harris, J. M. Reduction of fibrinogen adsorption on PEG-coated polystyrene surfaces. *J. Biomed. Mater. Res.* **1992**, *26*, 779–790.
- (54) McPherson Timothy, B.; Lee Samuel, J.; Park, K. Analysis of the Prevention of Protein Adsorption by Steric Repulsion Theory. In *Proteins at Interfaces II*; American Chemical Society: Washington, DC, 1995; Vol. 602, pp 395–404.
- (55) Prime, K.; Whitesides, G. Self-assembled organic monolayers: model systems for studying adsorption of proteins at surfaces. *Science* **1991**, *252*, 1164–1167.
- (56) Schubert, M. Another century of ellipsometry. *Ann. Phys.* **2006**, *15*, 480–497.
- (57) Xia, B.; Upadhyayula, S.; Nuñez, V.; Landsman, P.; Lam, S.; Malik, H.; Gupta, S.; Sarshar, M.; Hu, J.; Anvari, B.; Jones, G.; Vullev Valentine, I. Amyloid histology stain for rapid bacterial endospore imaging. *J. Clin. Microbiol.* **2011**, *49*, 2966–2975.
- (58) Thomas, M. S.; Nuñez, V.; Upadhyayula, S.; Zielins, E. R.; Bao, D.; Vasquez, J. M.; Bahmani, B.; Vullev, V. I. Kinetics of Bacterial Fluorescence Staining with 3,3'-Diethylthiacyanine. *Langmuir* **2010**, *26*, 9756–9765.
- (59) Özdemir, C.; Güner, A. Solution thermodynamics of poly(ethylene glycol)/water systems. *J. Appl. Polym. Sci.* **2006**, *101*, 203–216.
- (60) Luzinov, I.; Julthongpipit, D.; Malz, H.; Pionteck, J.; Tsukruk, V. V. Polystyrene layers grafted to epoxy-modified silicon surfaces. *Macromolecules* **2000**, *33*, 1043–1048.